Characterizing microstructure of refractory porous materials

XIN CHEN, DAYAKAR PENUMADU*
Civil and Environmental Engineering Department, University of Tennessee, 223 Perkins Hall, Knoxville, TN 37996, USA
E-mail: dpenumad@utk.edu

Liquid Expulsion technique was used in this study to quantify the transport properties and microstructure of a refractory coating used in the Lost Foam Casting process. The pore size information obtained from the Liquid Expulsion Method is found to be well correlated with the transport properties of the porous coating material. For manufacturing process control, the viscosity of these coating slurries prior to its application on expanded polystyrene foam is often reduced by dilution with water and/or using a dispersant. In this paper, the effects of diluting or dispersing the slurry on the microstructure and transport properties of the dried refractory coatings are evaluated. Results show that the dilution and dispersion have opposing influences on the pore size and transport properties. Adding dispersant was found to reduce the transport properties of the refractory coatings significantly, potentially leading to defects in metal castings. The pore characterization technique developed in this paper is also used to determine the effects of drying methods (oven versus air dry) on the pore size and transport properties.
© *2006 Springer Science + Business Media, Inc.*

1. Introduction

Microstructure is one of the important factors governing the transport behavior of a porous medium, such as its Darcy coefficient, and the related properties such as thermal conductivity and density. Therefore, it is necessary to understand the microstructure of porous media such as the pore size and distribution. A number of experimental techniques and commercial instruments are available for determining pore size distribution, such as: Scanning Electron Microscopy (SEM), Mercury Intrusion Porosimetry (MIP), the Bubble pressure and gas transport method, Gas Absorption, and the Liquid Displacement Method (LDM) [1–3]. In a porous medium that originates from drying of slurries, voids exist as the spaces between the particles. Some of them are connected to each other, forming the channels for the air/liquid to pass through, which are considered effective pores. Some voids are isolated and not open to the atmosphere and are considered ineffective pores. For a porous medium, the transport properties are particularly related to the effective pores in the porous structure. Therefore, the effective pore size and pore size distribution are important for understanding the physical behavior of a porous medium.

In this paper, a technique known as water-expulsion porosimetry, also called the Liquid Expulsion method, proposed by Gelinas and Angers [4], was used to characterize the microstructure information of ceramic coatings. The results from this study are compared with those obtained using the mercury intrusion method. The major purpose of this paper was to investigate the applicability of such a technique for refractory porous materials used in foundry industries. The relationship between the experimentally determined pore size information and the corresponding transport properties of these refractory porous materials was also investigated. In addition, this paper also studied the influences of dilution/dispersion and different drying procedures (oven and air) on the microstructure and transport properties of lost foam casting coatings.

2. Background

In this work, the applicability of the Liquid Expulsion Method was investigated to evaluate the microstructure of refractory coatings used in a relatively new metal casting technique called Lost Foam Casting (LFC). LFC, also known as Expandable Polystyrene Casting (EPC), is a

popular casting method being used as a replacement for the conventional casting techniques to obtain near net-shape metal castings. The casting products are produced by pouring molten metal into a foam pattern that is coated with refractory material, which is then surrounded and compacted by unbonded sand through vibration. The foam pattern degrades into gas and vents into the loose sand after the molten metal is introduced, and the metal then fills the foam pattern to get the final product. In order to ensure the adequate thermal properties of filling molten metal and the venting of pyrolysis products, the EPS foam pattern is coated with refractory slurry. The refractory coating has to be strong enough to resist the pressure to avoid metal penetration defects. At the same time it should have adequate transport properties to allow the escape of the degraded materials (styrene gas predominantly) to avoid defects in the metal casting, such as mis-runs, folds, and porosity [5–14]. These refractory coatings are initially applied to the polystyrene foam patterns in a slurry stage and are allowed to dry. The microstructure of these porous materials is complex and affects the mechanical strength and transport properties of the refractory coating. Therefore, the characterization of pore size and pore size distribution is important for developing new and novel coatings and also for manufacturing process control in LFC foundries.

3. Experiments

Mercury Intrusion Porosimetry has been widely used in the past as a technique to characterize the microstructure of porous media [15–18]. Thus, this paper includes comparison results from the Mercury intrusion method and the Liquid Expulsion Method developed in this study.

Non-wetting material such as mercury is used in the Mercury Intrusion Method. As a non-wetting material, mercury will not spontaneously wet most surfaces or enter the pores in a solid because of its high surface tension. In order to fill the pores with mercury, external pressure is needed to force mercury into the pores. If a cylindrical pore model is assumed, the relationship between pressure and pore size is given by the Washburn equation [20]. Because the sizes of the pores that can be filled with mercury are inversely proportional to the applied pressure, mercury intrudes the bigger pore first and, successively, the smaller ones with increasing pressures. Thus, the pore size distribution can be determined by monitoring the volume of intruded mercury as a function of increasing applied pressure [19]. In this study, the pore size analysis was evaluated by a Poromaster 60 (Quantachrome Corporation), which can generate a maximum intrusion pressure of 413.7 Mpa for pore size analysis from approximately 950 microns to 0.0036 microns equivalent pore diameter.

According to Hernandez *et al*. [21], Bechhold *et al*. [22] were the first to use the Liquid Expulsion Method to evaluate pore size by measuring the pressure to blow air through water-filled membranes. Lately, the Liquid

Expulsion Method has been modified in several ways and adopted by ASTM and British Standards Institution for determining pore size characteristics of porous materials [23–25]. The Liquid Expulsion Method uses a wetting liquid instead of a non-wetting liquid to measure pore size. The wetting liquids will spontaneously flow into pores in the solid, and work is required to remove the wetting liquid from the pores. A relationship between the applied pressure, the flow rate of the air through saturated porous materials, and pore size can be used to estimate the pore size distribution of porour materials.

In this work, the pore size analysis was investigated by a Capillary Flow Porometer (Porous Material Inc.) [26] and a portable automated porometry system developed at the University of Tennessee [27], which can generate pressure to 3.45 MPa for pore size analysis from over 500 micron to 0.013 micron pore diameter. The sample was soaked in a wetting liquid (Galwick) of low surface tension ($\gamma = 0.0156$ N/m), low vapour pressure and low reactivity. The saturated sample was then subjected to increasing pressure. As the pressure increases, it will reach a point where applied pressure overcomes the surface tension of the liquid in the largest pores and will push the liquid out. This minimum pressure required to push the liquid out from largest effective pore and make the first detectable flow is called "bubble pressure," which is used to calculate the "bubble pore size"—the maximum pore size. Continuing to increase the pressure further allows the air to empty smaller pores. By testing the sample both in the dry condition and the saturated (wet) condition, it is possible to obtain a plot of flow rate versus applied pressure, as illustrated in Fig. 1. When the applied pressure empties all of the pores saturated with Galwick, the flow rate vs. pressure curve (flow-pressure curve) will return to the flow-pressure curve of the dry sample. By comparing the gas flow rate of both a wet and dry sample at the same pressure, the percentage of the flow passing through the sample caused by the pores
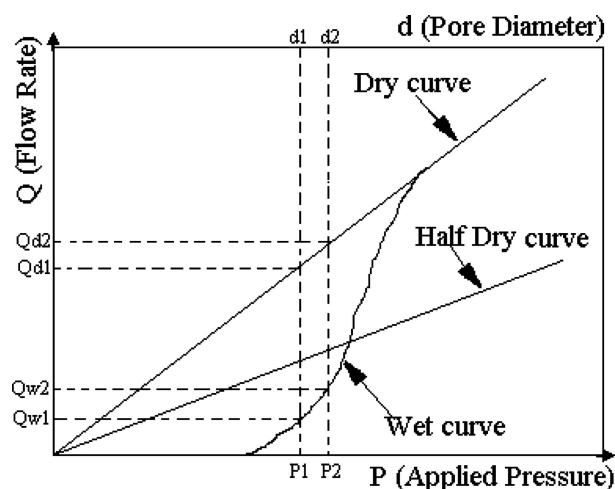

Figure 1 Typical flow rate versus applied pressure for wet and dry samples.

larger than or equal to the specified size can be calculated as:

$$\%\text{Filter Flow Percentage} = \frac{\text{wet\_flow\_rate}}{\text{dry\_flow\_rate}} \times 100 \quad (1)$$

The flow caused by the pore size in a certain range between $d1$ and $d2$ can also be calculated as

$$\%\text{Filter Flow Percentage} (d_2 - d_1)$$
$$= \left(\frac{Q_{w2}}{Q_{d2}} - \frac{Q_{w1}}{Q_{d1}} \right) \times 100 \quad (2)$$

The mean flow pore size is determined by the intersection of a wet flow-pressure curve and a half dry flow-pressure curve, where the flow rate through the wet sample is one half of the flow rate through the dry sample at the same pressure. The corresponding pressure is called the mean flow pressure.

3.1. Evaluation of transport properties
Transport properties of porous materials are generally characterized using their permeability coefficients. In this work, Forchheimer's equation [28] is used to calculate the permeability coefficient of the refractory LFC coatings. Forchheimer's equation has proven to be more appropriate for estimating the transport properties of the refractory LFC coating in a relatively wide range of applied pressures [27], since it includes parabolic parts in the equation by considering the influence of inertia and turbulence. Forchheimer's equation can be written as

$$\frac{P_i^2 - P_0^2}{2PL} = \frac{\mu}{k_1} v_s + \frac{\rho}{k_2} v_s^2 . \quad (3)$$

where ρ is the fluid density; constant k_1 and k_2 are the Darcian (viscous) permeability and non-Darcian (inertia) permeability coefficients, respectively; v_s is the fluid velocity, calculated by dividing the exit volumetric flow rate Q by the cross-sectional area A. μ is the viscosity of the fluid. P_i is the pressure at the sample entrance; P_o is the pressure at the sample exit; and P is the fluid pressure at which Q and μ are measured or calculated. In general, P equals to P_o. L is the coating thickness. In this research, permeability coefficients were obtained by fitting experimental data through the least squares method to Equation 3.

The term "flow factor" as defined in Equation 4 was developed in this study for transport property comparison purposes for coating materials of differing composition. It not only considers the effect of the material's microstructure (for example, Darcian permeability coefficient) but also considers another key factor controlling the coating's transport properties, its average thickness. This "flow factor" can be used to compare different types of coatings'

transport properties at the same differential pressure. A large "flow factor" indicates high transport capability.

$$\text{Flow Factor} = \frac{k_1}{L} \quad (4)$$

3.2. Sample preparation
In this work, fourteen different types of Lost Foam Casting refractory coating have been investigated. These slurries were produced for two major automotive Powertrain LFC foundries by three commercial suppliers. These coating slurries were used for different parts, such as an engine block or a cylinder head. These water-based coatings consist of silica, mica, binding clay, synthetic ceramic particles, and some latex binders with solids percentages of 40 to 62%.

In order to investigate the dilution and dispersion effects, 5% of water by volume was added to the synthetic coating H to obtain the diluted synthetic coating H. Similarly, 1% of dispersant (CALGON) by weight was added to the synthetic coating H to obtain the dispersed synthetic coating H. In addition, some data collected from a manufacturing facility dealing with casting 4 cylinder blocks and head are also included in this study.

The coating samples were obtained by dipping a 100×100 stainless steel mesh disc of 6.51 cm diameter into the coating slurries, whose rheological properties were well controlled and studied. The steel mesh has very high permeability, which will not affect the measuring results for the coating permeability. The dipped coating discs were then dried at room temperature. After drying, the thickness of each coating was measured by using a 0–2.54 cm micrometer (with a resolution of 0.00254 mm). In order to investigate the oven-dry effects on the coating permeability, samples of coatings B and H that were dried at room temperature (25°C) and in an oven at 60°C were individually prepared for comparison purposes.

4. Results and discussion
4.1. Comparison of the Mercury Intrusion Method and the Liquid Expulsion method
Fig. 2 compares the pore side distributions measured by the Mercury Intrusion Method and Liquid Expulsion Method for coatings B and H. It shows that a majority of the intruded mercury (87%) volume for coating H correspond pores with a diameter of 5 um or higher (up to 150 um); while for coating B the pores with a diameter larger than 5 um correspond to only 45% intrusion of volume. This indicates that the pore diameters of coating B are smaller compared to the pore diameters of coating H. Based on theory discussed earlier, the filter flow percentage can be calculated as shown in Fig. 2 according to Equation 1, which shows that the detectable effective pores were smaller than 15 um for both coatings B and H. It also shows that the pores of coating B are finer than those of coating H. Fig. 3 shows the flow
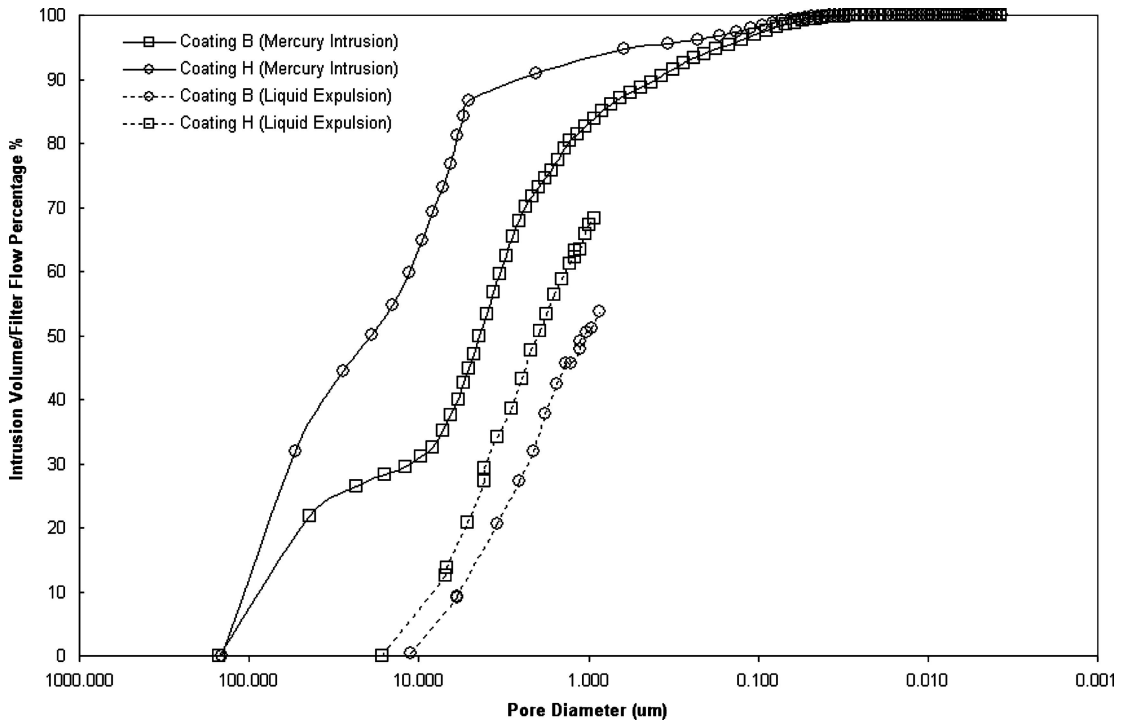
Figure 2 Comparison of pore size distributions determined by Mercury Intrusion Method and Liquid Expulsion Method.
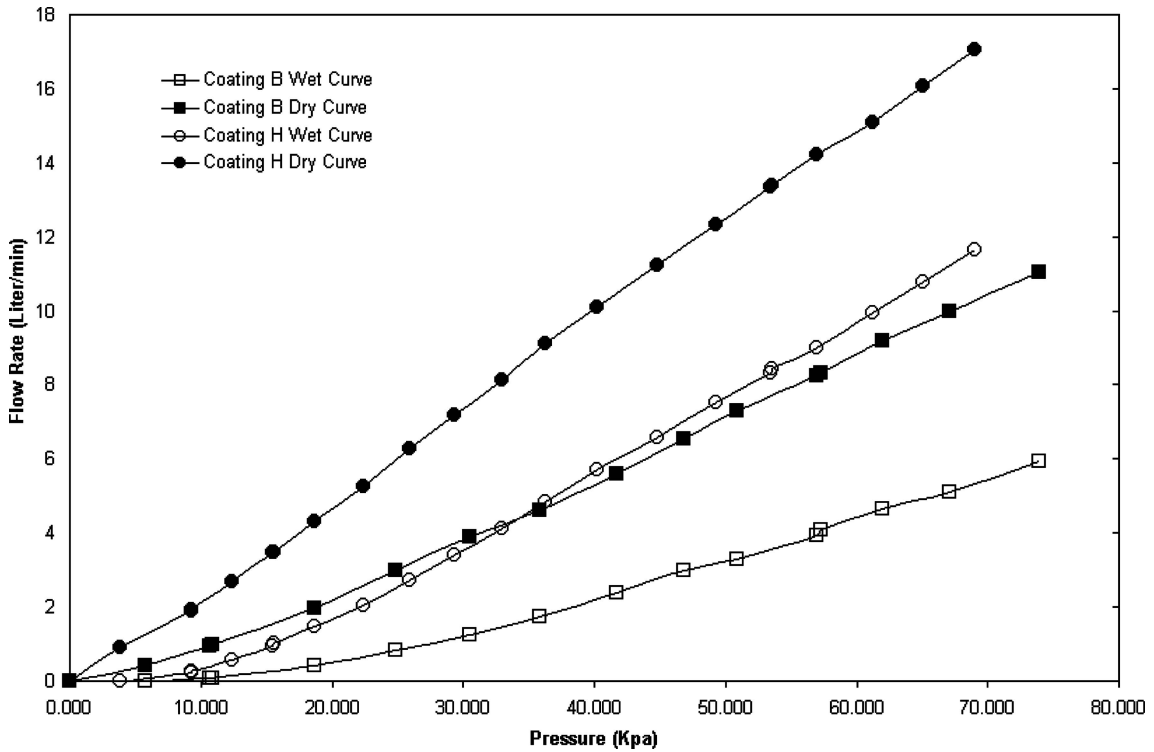

Figure 3 Flow rate against applied pressure curves for coating B and H.

rate versus applied pressure curves obtained by the Liquid Expulsion Method for these two coatings (B and H). The air flow rate versus differential pressure data clearly show that coating H is more permeable than coating B. It can also be seen that the flow rate of the wet sample increases with increasing pressure as pores saturated initially with Galwick are being emptied with higher gas pressure. In this study, considering the strength of coating samples, the maximum pressure applied on the samples was set at 76 kpa. Although 76 kPa was not high enough to expel Galwick from the wet sample pores completely, it was sufficient to obtain the bubble pore

size and the mean pore size information, with the measured pressure range being identical for both coatings. Table I lists the comparison of pore size determined by the Mercury Intrusion Method and the Liquid Expulsion Method. It can be seen that the flow factor is a valuable indicator to evaluate the transport properties of the refractory coatings. There are differences in microstructure information (pore size) determined by the Mercury Intrusion Method and the Liquid Expulsion Method, in that the Mercury Intrusion Method shows relatively larger pores than those detected by the Liquid Expulsion Method.

It is not surprising that the results from the Mercury Intrusion Method and the Liquid Expulsion Method are not in quantitative agreement. In the Mercury Intrusion Method, when pressure increases, the mercury will intrude the bigger pores first and then the smaller pores, which does not take into consideration whether the pores are permeable to liquid or not. Therefore, the non-effective (blind) pores may be detected in the Mercury Intrusion Method, thereby contributing to the calculation of the pore size distribution. However, the Liquid Expulsion Method only measures the effective pores, which means the pore size distribution obtained by the Liquid Expulsion Method only accounts for the permeable pores. For this reason, the Liquid Expulsion Method will be more suitable for the study of materials' transport properties, which is critical for refractory coating materials used in LFC foundries. In reality, most of the pores in a porous medium will not be made of straight tubes of varying diameters. The typical pore channel shapes for a given coating are qualitatively illustrated in Fig. 4. Pore type *d* shown in Fig. 4 is a blind pore, which will not contribute to the transport properties; however, the Mercury Intrusion Method will still measure it. The Liquid Expulsion Method only detects those pores which are totally open through the coating thickness; therefore, pores *a–c* in Fig. 4 will be detected only if the pressure reaches a certain point to push the liquid out through the constricted portion of the pore channels. Thus, the pore size measured by the Liquid Expulsion Method is the smallest diameter of the whole pore channel. However, the Mercury Intrusion Method may consider such a pore as several

different-sized pores. For example, pore *a* and *b* will be individually considered as 3 pores of different sizes. Pore *c* might be detected as dozens of pores varying in size. In order to analyze small pores, very high pressure is applied in the Mercury Intrusion Method, which may distort the microstructure of tested samples [21]. The high pressure may deform some pores and even make them collapse. In addition, the Mercury Intrusion Method has a relatively low resolution at larger pore sizes [29]. Measurements of the maximum pore size (bubble pore size) by the Mercury Intrusion Method will not be as accurate as those obtained from the Liquid Expulsion Method. The differences mentioned above explain the reasons that the Mercury Intrusion Method might give relatively larger size ranges for pores than those detected by the Liquid Expulsion Method.

Although differences exist between the Mercury Intrusion Method and the Liquid Expulsion Method, both methods tend to indicate that coating H had relatively larger pores than coating B, which is also confirmed by images obtained from the Scanning Electron Microscope. Comparing Figs 5 and 6, it can be seen that the surface of coating B is fairly smooth, while the surface of coating H is particularly rough. It is reasonable to assume that particle shape is one of the factors influencing pore size distribution. Coating B is mainly based on mica, which is flaky; while the majority of particles in coating H are silica, which is bulky. Bulky particles might more easily tend to construct voids between particles, which form tunnels for gas/liquid to pass through. Since any porous material may contain both flow-through pores and blind-pores, the maximum of the PSD obtained from liquid-expulsion porometry is usually shifted toward smaller pores as compared with mercury intrusion technique [30].

4.2. Pore shape factor
From Figs 5 and 6, it can also be seen that most of the pores do not have cross-section that mimics a circle, an implicit assumption for interpretation. Therefore, a pore shape factor is often proposed to consider the non-circular cross section. If the pore section is considered to be ellip-

TABLE I Comparison of pore size determined by Mercury intrusion method and liquid expulsion method

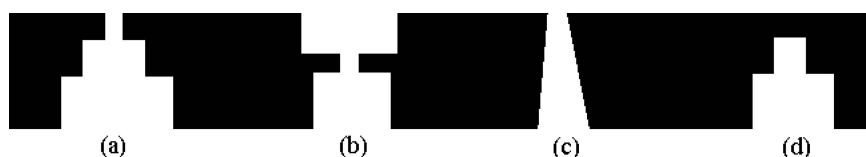| Sample	Thickness (mm)	Bubble pressure (KPa) LEM	Bubble pore size (um) LEM	MIP	Mean pore size (um) LEM	MIP	Permeability coefficient (Darcy)	Flow factor (Darcy/mm)
Coating B	0.559	5.74	11.15	149.00	1.06	4.41	0.013	0.022
Coating H	0.503	3.86	16.59	146.00	2.01	18.90	0.027	0.053

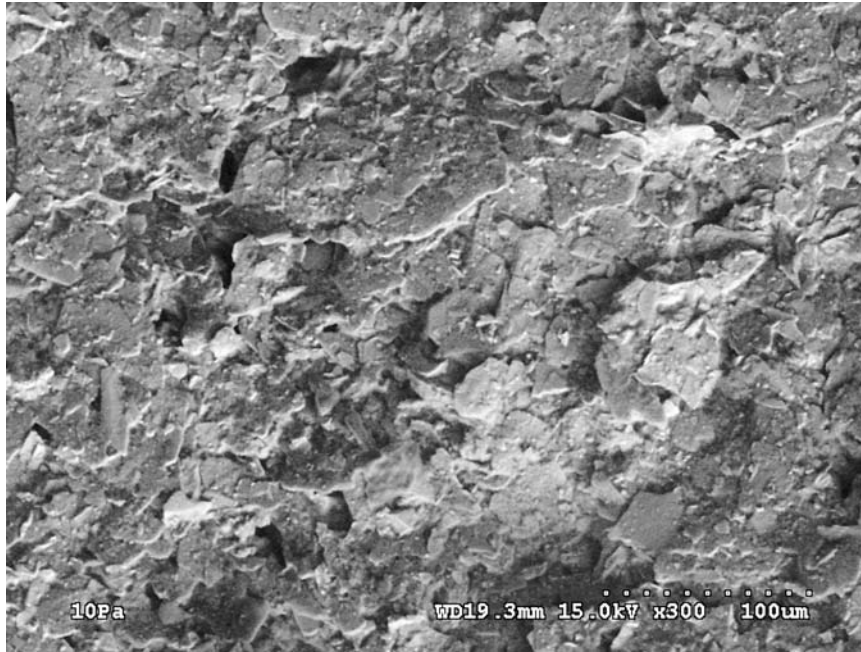*Figure 4* Influences of pore channel shape on pore size determination.

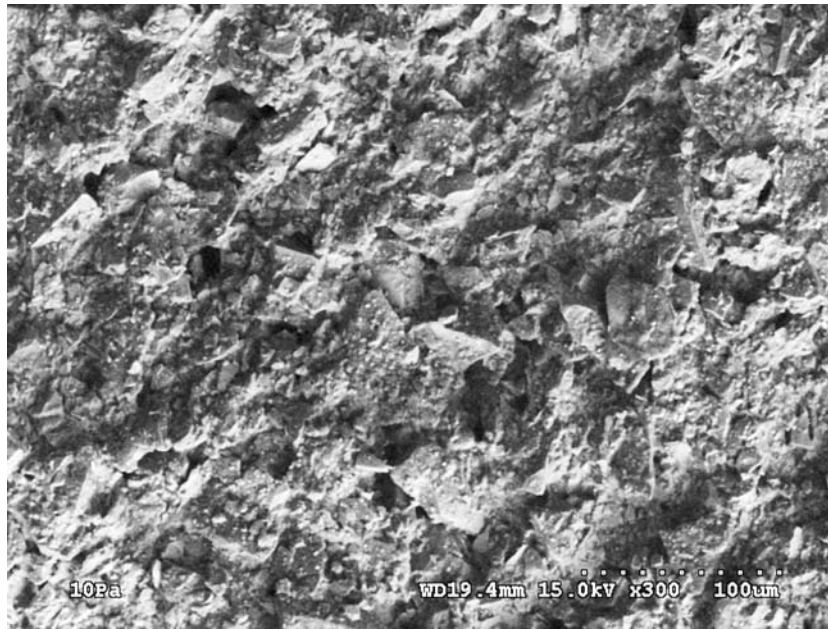*Figure 5* Surface microstructures image of coating B.

Figure 6 Surface microstructure image of coating H.

tical with minor axis d and major axis nd, the following relationship exists:

$$\frac{dS}{dV} = \sqrt{\frac{1}{d} \cdot \frac{8 \cdot (1 + n^2)}{n^2}} \qquad (5)$$

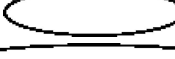The pore shape factor can be defined as

$$\lambda = \frac{d}{D} = \sqrt{\frac{1 + n^2}{2 \cdot n^2}} \qquad (6)$$

Some typical values of the pore shape factor are listed in Table II. In the following part of this paper, all the pore sizes have been assumed to have n value of 7, and thus the results based on cylindrical pore shape are multiplied using a pore shape factor of 0.715.

4.3. Correlation between bubble pore size, mean pore size and flow factor

In this work, it was found that useful relationships exist between bubble pore size, mean pore size and flow factor. As shown in Fig. 7, the mean pore size increases as

TABLE II Pore shape factor

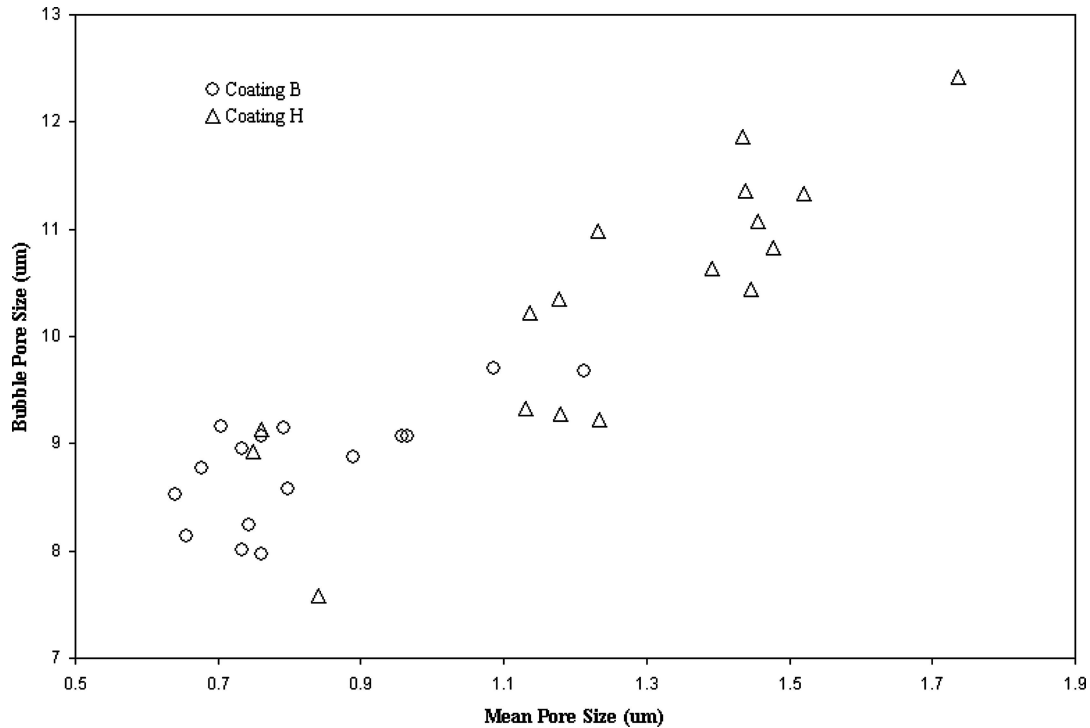| Pore cross section	n	Shape factor λ $(d = \lambda D)$
	1	1
	2	0.791
	4	0.729
	7	0.714

Figure 7 Bubble pore size vs. mean pore size for coating B and H.

the bubble pore size increases for coating B and H. The data collected at a manufacturing facility using the liquid expulsion technique described in this paper for coatings I, LB, LH and T are shown in Fig. 8. These data show that mean pore size increases with the increased bubble pore size. However, coating LH did not demonstrate this trend significantly, which might be attributed to the bulky-shaped particles in coating LH. The majority of the particles in coating I, LB and T were flaky-shaped particles, mica. During the dipping and drying process, the flaky-shaped particles might demonstrate relatively organized orientations, which might cause the consistent trend between bubble pore sizes and mean pore sizes. However, coating LH mainly consisted of bulky-shaped particles, silica. During the dipping and drying process, these bulky-shaped particles might have all kinds of orientations, which might disrupt the trend between bubble pore sizes and mean pore sizes.

A strong relationship was also observed between flow factor, bubble pore size and mean pore size as shown in

Fig. 9 through Fig. 13, which indicates that it is possible to predict the transport properties (flow factor in this study) by measuring the microstructure information (pore size in this study) of refractory LFC coatings. As shown in Fig. 11, linear regression gives $R^2 = 0.81$ for an assumed linear relationship between flow factor and mean pore size for coatings B and H, which suggests that 81% of the changes in flow factor can be explained by the changes of mean pore size for the samples prepared and studied in the laboratory of the authors. In contrast, the data collected at a manufacturing process control facility for 8 types of commercial refractory LFC coatings as shown in Fig. 12 seem to fit two linear trends, both of which demonstrate fairly good linearity ($R^2 \geq 0.81$). In addition, the linear regression equations obtained for 8 types of commercial refractory LFC coatings seem to work fairly well for coating I, LB, LH and T, which are the refractory LFC coatings currently used at this metal casting facility. Although $R^2 = 0.32$ is relatively poor for coating LH, the variations between the predicted flow factor using the
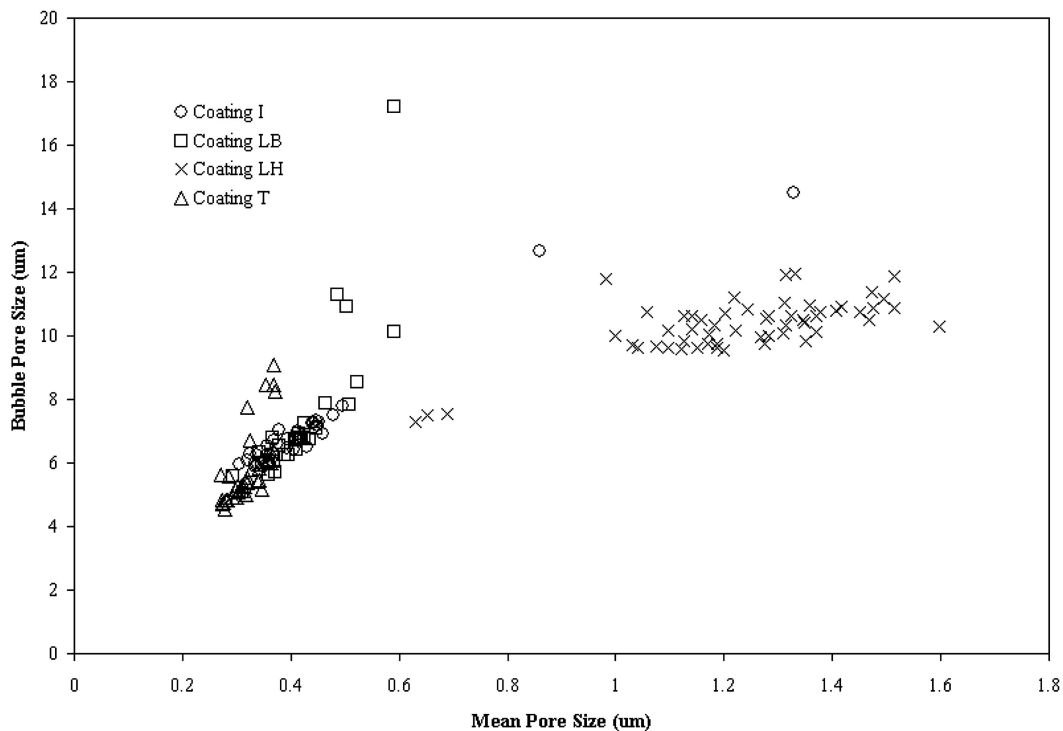
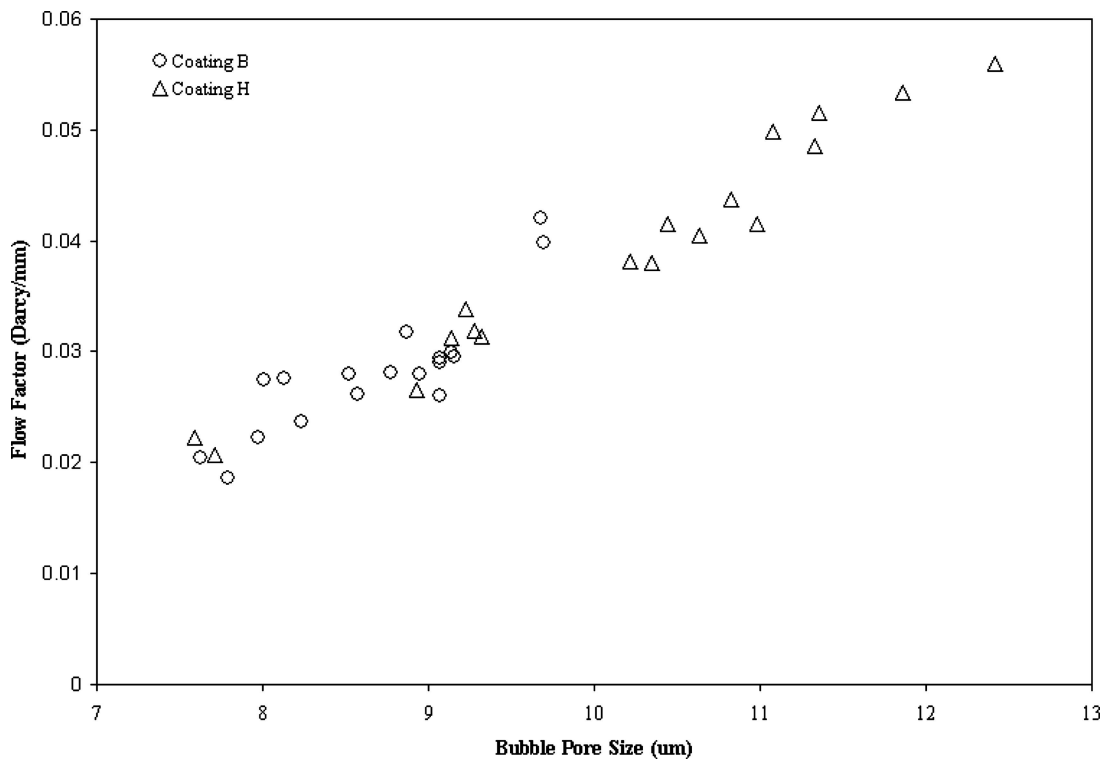*Figure 8* Bubble pore size vs. mean pore size for coating I, LB, LH and T.

Figure 9 Flow factor vs. bubble pore size for coating B and H.

linear equation in Fig. 12 and the measured flow factor are within ±30%, as shown in Fig. 14. The reason for the inconsistent behavior for coating LH is not clear yet; however, the overall results do imply that the linear relationship between flow factor and mean pore size does exist but might not be able to be predicted by a unique equation that is universal to coating component variations. The analysis of the bubble pore size and mean pore size data provides valuable insight for understanding a relationship between the microstructure and the transport properties of these complex multi-component refractory LFC coatings.
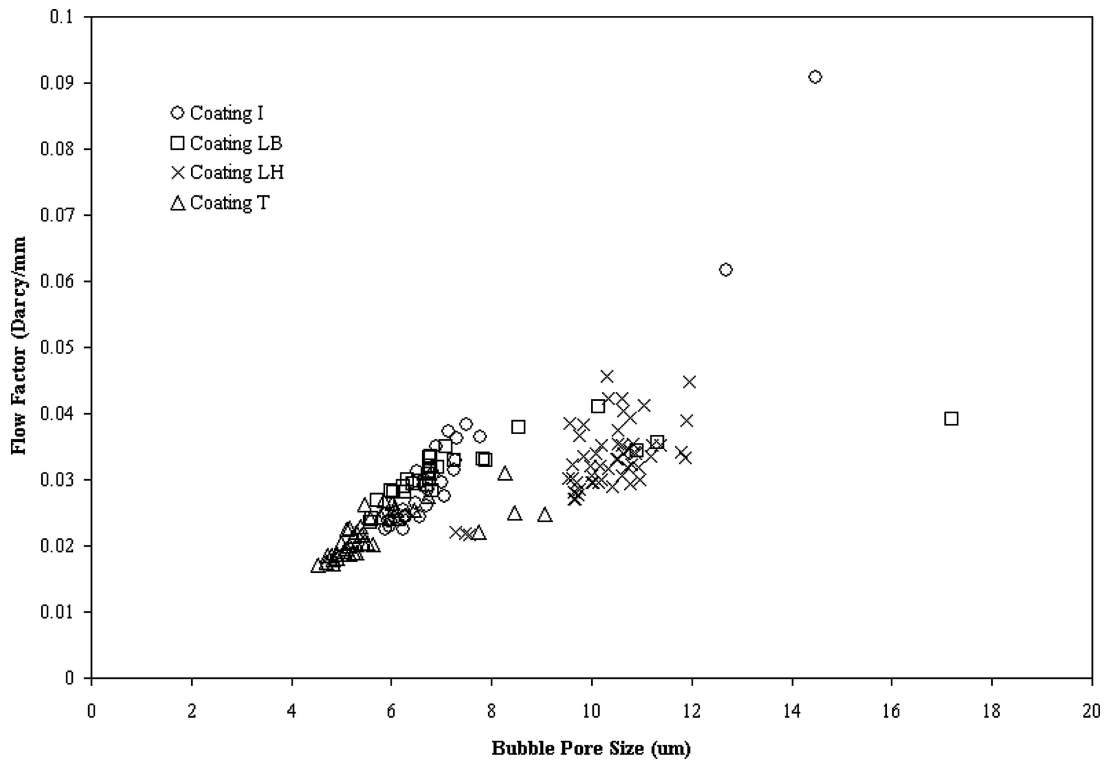
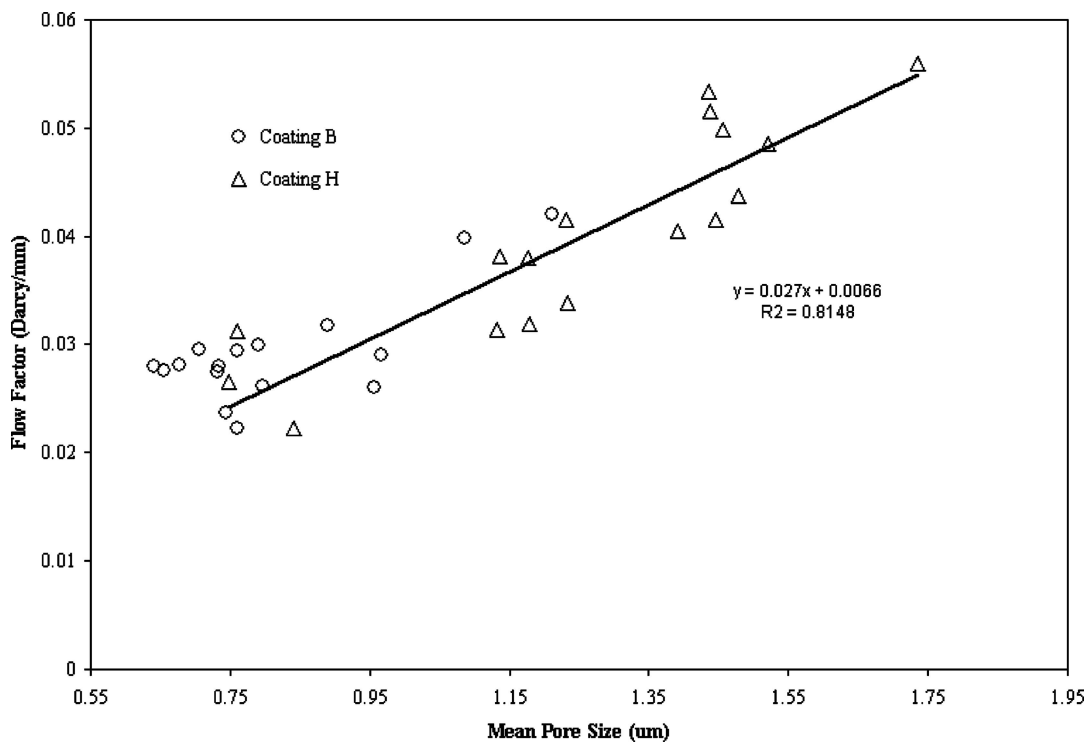*Figure 10* Flow factor vs. bubble pore size for coating I, LB, LH and T.

Figure 11 Flow factor vs. mean pore size for coating B and H.

4.4. Effect of dilution and dispersion

In LFC foundries, the coating slurries shipped from suppliers are normally concentrated, and have a viscosity higher than what is used for actual coating purposes. Generally, operators in LFC foundries will add water and/or dispersant to these concentrated slurries to obtain desirable rheological data (flows well, does not drip, and levels without sagging). Therefore, it is essential
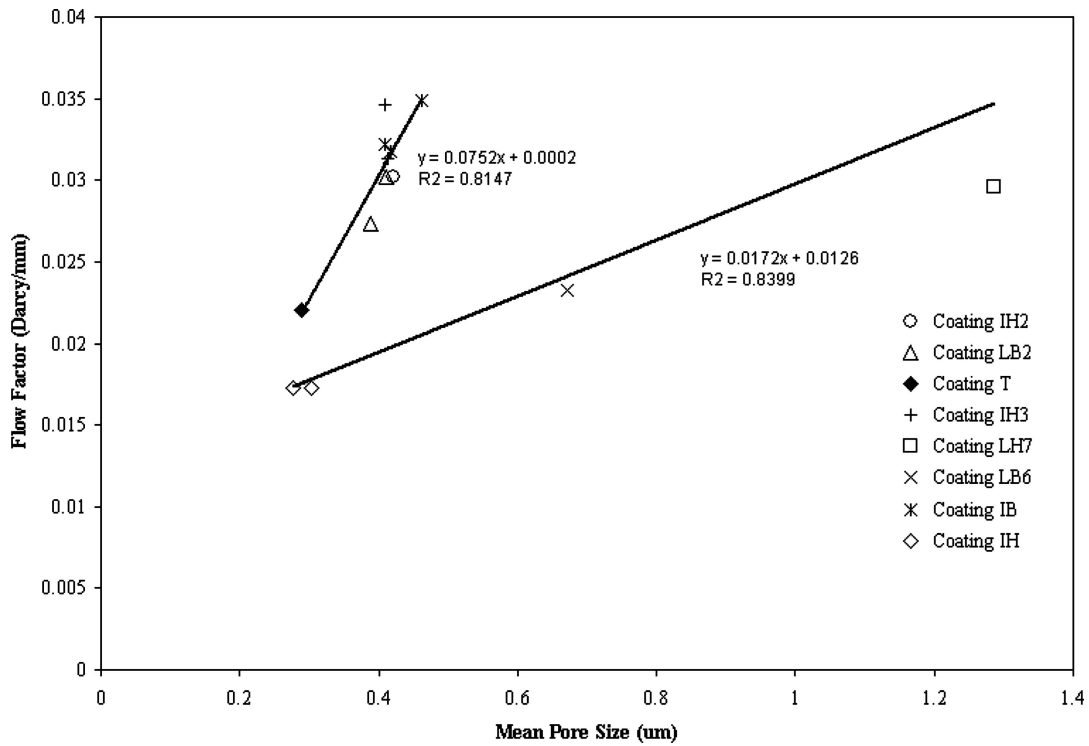
Figure 12 Flow factor vs. mean pore size for various coatings.

to investigate the effects of dilution and dispersion on the transport properties of refractory coatings. In this study, 5% of water by volume was added to the synthetic coating H to obtain diluted synthetic coating H.

Similarly, 1% of dispersant (CALGON) by weight was added to the synthetic coating H to obtain the dispersed synthetic coating H. Results shown in Table III suggest that adding dispersant may reduce the bubble pore size as
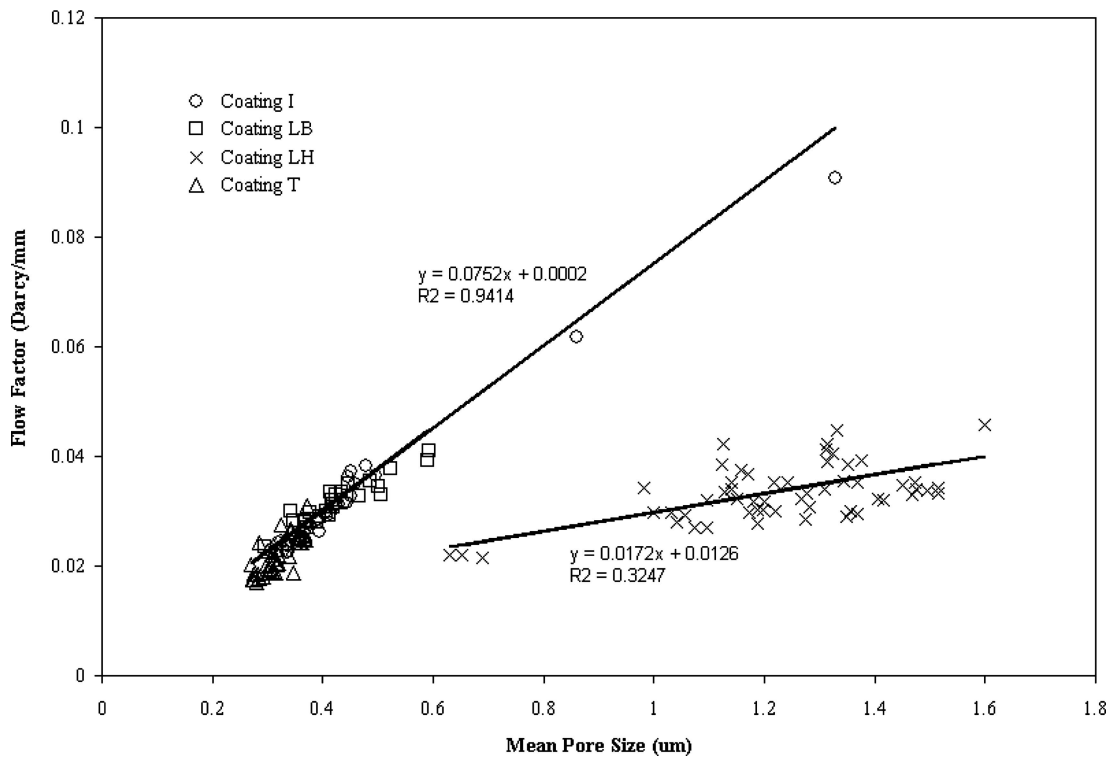

Figure 13 Flow factor vs. mean pore size for coating I, LB, LH and T.
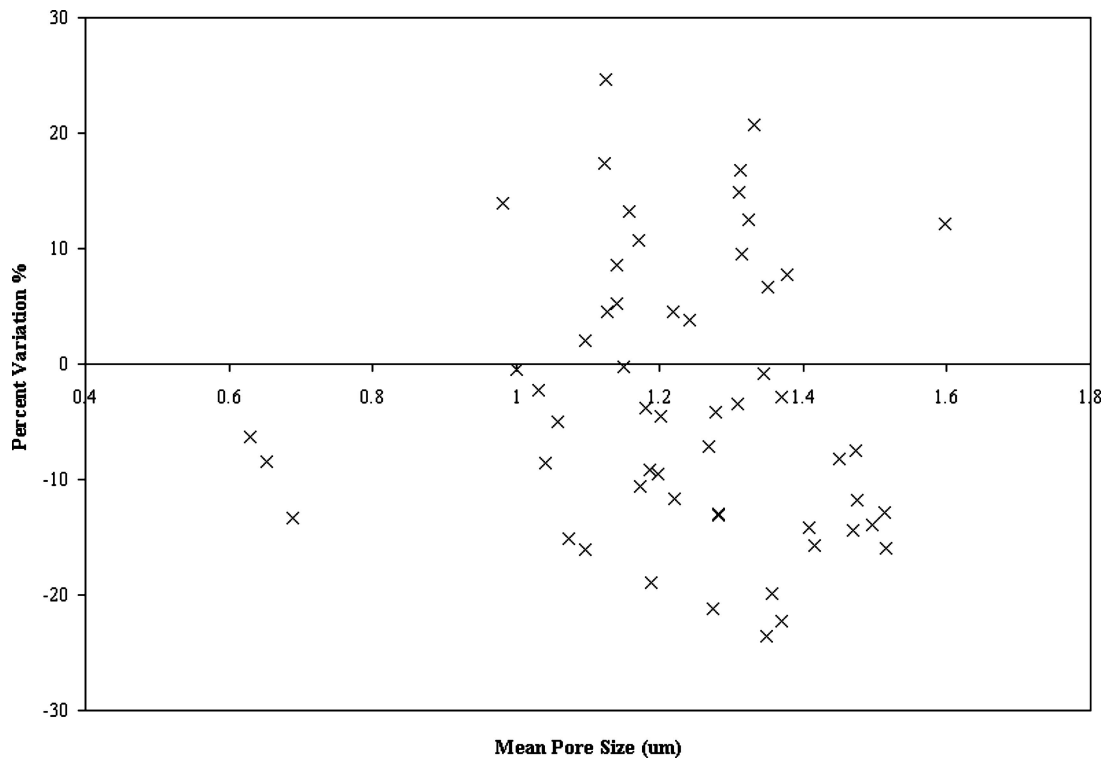
3412

Figure 14 Percent variance of predicted flow factor for coating LH.

well as mean pore size; correspondingly, the flow factor declines. In contrast, adding only water tends to increase the bubble pore size and mean pore size, which simultaneously raises the flow factor. This study suggests that adding dispersant will reduce the pore size and transport properties although adding dispersant might get similar rheological performance (viscosity values at a target rpm) as can be obtained by simply diluting with water.

4.5. Effect of drying process
Generally, oven and air drying are two practical approaches used in LFC foundries. Table IV shows the comparison data for two drying techniques for the two coatings B and H. Oven drying at 60°C slightly increases the bubble pore size as well as the mean pore size; however, it does not significantly affect the transport properties (flow factor). Therefore, it is reasonable to conclude that oven versus air drying processes do not have substantial differences on the pore size and transport properties. It will be interesting to perform similar studies for other drying techniques such as freeze and critical point drying. This could shed new light on obtaining desirable properties by varying the drying process. The equipment and procedures developed in this study will be valuable for generating such data.

5. Conclusion
In this study, the applicability of the Liquid Expulsion Method was investigated for refractory LFC coatings. The results have shown that the Liquid Expulsion Method is more suitable to characterize the "effective pore" struc-

ture. Compared to the Mercury Intrusion Method, the Liquid Expulsion Method has the following advantages: (1) No toxic liquid (Mercury) is used; (2) It is a non-destructive test; the sample is not damaged or contaminated; (3) Only effective pores are detected; therefore, this technique is more appropriate to characterize the microstructure of porous material for transport behavior. Results from this study have also suggested that useful relationships can be derived between flow factor, bubble pore size and mean pore size. This has implications for using fewer variables such as a bubble pore size and mean pore size as good indicators to understand the relationship between the microstructure and the transport properties of refractory LFC coatings. The present study also found that the dilution and dispersion have opposing influences on the pore size and permeability. The dispersant should be used cautiously in LFC foundries because it might reduce the transport properties of the refractory coatings. No significant differences between oven and air dry processes were found for interpreted and measured parameters using Liquid Expulsion Method for refractory coatings used in Lost Foam Casting.

SYMBOLS LIST
d_1 pore diameter corresponding to applied pressure P_1

d_2 pore diameter corresponding to applied pressure P_2

Q_{w1} flow rate measured for wet sample corresponding to applied pressure P_1

TABLE III Dilution and dispersion effects on pore structure

Sample	Thickness (mm)	Bubble pore size (um)	Mean pore size (um)	Permeability coefficient (Darcy)	Flow factor (Darcy/mm)
Coating H diluted	0.432	16.23	1.51	0.028	0.065
Coating H dispersed	0.301	10.57	0.83	0.010	0.035
Coating H original	0.436	11.10	1.32	0.020	0.047

TABLE IV Comparison of oven-dry and room-dry process results

Sample	Thickness (mm)	Bubble pore size (um)	Mean pore size (um)	Permeability coefficient (Darcy)	Flow factor (Darcy/mm)
Oven-dry coating B	0.480	8.75	0.85	0.016	0.033
Room-dry coating B	0.479	8.27	0.75	0.016	0.033
Oven-dry coating H	0.502	10.55	1.19	0.024	0.048
Room-dry coating H	0.494	9.71	1.10	0.020	0.040

Q_{w2} flow rate measured for wet sample corresponding to applied pressure P_2

Q_{d1} flow rate measured for dry sample corresponding to applied pressure P_1

Q_{d2} flow rate measured for dry sample corresponding to applied pressure P_2

P_1 applied pressure at point 1

P_2 applied pressure at point 2

ρ fluid density

k_1 Darcian (viscous) permeability coefficient

k_2 non-Darcian (inertia) permeability coefficient

v fluid velocity

Q volumetric flow rate

A sample cross-sectional area

μ the viscosity of the fluid

P_i the pressure at the sample entrance

P_o the pressure at the sample exit

P the fluid pressure at which Q and μ are measured or calculated

L sample thickness

dS differential of pore area

dV differential of pore volume

d minor axis of elliptical or pore diameter

n the ratio of major axis to minor axis

λ Pore Shape Factor

Reference
1. S.-I. NAKAO, *J Membr Sci* **96** (1994) 131.
2. Y. LEE, J. JEONG, I. J. YOUN and W. H. LEE, *ibid.* **130** (1997) 149.
3. C. ZHAO, X. ZHOU and Y. YUE, *Desalination* **129** (2000) 107.
4. C. GELINAS and R. ANGERS, *Am. Ceram. Soc. Bull.* **65** (1986) 1297.
5. J. R. BROWN, *Met. Mater.* **8** (1992) 550.
6. C. A. GORIA, G. CAIRONI and G. TOSI, *Trans Amer Foundrymen's Soc* **94** (1986) 589.
7. S. SHIVKUMAR, L. WANG and D. APELIAN, *J Mater.* **November** (1990) 38.
8. Y. SUN, H.-L. TSAI and D. R. ASKELAND, *Trans Amer Foundrymen's Soc.* **100** (1992) 297.
9. H. LITTLETON, B. MILLER, D. SHELDON and C. BATES, *Found Manag & Technol* **125** (1997) 41.
10. J. LIU, C. W. RAMSAY and D. R. ASKELAND, *Trans Amer Foundrymen's Soc* **105** (1998) 419.
11. C. E. BATES, J. A. GRIFFIN and H. E. LITTLETON, "Expendable pattern casting, Casting defects manuals" (American Foundrymen's Society, 1994).
12. S. BENNETT, T. MOODY, A. VRIEZE, M. JACKSON, D. R. ASKELAND and C. W. RAMSAY, *Trans Amer Foundrymen's Soc* **108** (2000) 795.
13. M. A. TSCHOPP, Q. G. WANG and M. J. DEWYSE, *ibid.* **110** (2002) 1371.
14. J. LIU, C. W. RAMSAY and D. R. ASKELAND, *AFS Transactions* **139** (1997) 435.
15. ASTM-D4284, in "Standard Test Method for Determining Pore Volume Distribution of Catalysts by Mercury Intrusion Porosimetry", (ASTM Committee D-32 on Catalysts, Conshohocken, PA, 1994).
16. ASTM-D2873, in "Standard Test Method for Interior Porosity of Poly(Vinyl Chloride) (PVC) Resins by Mercury Intrusion Porosimetry" (ASTM Committee D-20 on Plastics, Conshohocken, PA, 1994).
17. ASTM-D4404, in "Standard Test Method for Determining of Pore Volume and Pore Volume Distribution of Soil and Rock by Mercury Intrusion Porosimetry" (ASTM Committee D-18 on Soil and Rock, Conshohocken, PA, 1994).
18. DIN66133, in "Determination of Pore Volume Distribution and Specific Surface Area of Solids by Mercury Intrusion (in German)" (Deutsches Institut Fur Normung e.V, 1993).

19. S. LOWELL and J. E. SHIELDS, in "Powder Surface Area and Porosity" (Chapman & Hall, New York, 1998).
20. E. W. WASHBURN, *Phys. Rev.* **17** (1921) 273.
21. A. HERNANDEZ, J. I. CALVO, P. PRADANOS and E. TEJE-RINA, *J Membr Sci* **112** (1996) 1.
22. H. BECHHOLD, M. SCHLESINGER, K. SILBEREISEN, L. MAJER and W. NURNBERGER, *Kolloid Z.* **55** (1931) 172.
23. ASTM-D6767-02, in "Standard Test Method for Pore Size Characteristics of Geotextiles by Capillary Flow Test" (ASTM Committee D35 on Geosynthetics, Conshohocken, PA, 2002).
24. ASTM-F316-03, in "Standard Test Method for Pore Size Characteristics of Membrane Filters by Bubble Point and Mean Flow Pore Test" (ASTM Committee D19 on Water, Conshohocken, PA, 2003).
25. BS-7591, in "Porosity and Pore Size Distribution of Materials: Part 4. Method of Evaluation by Liquid Expulsion" (British Standards Institution, 1993).
26. A. K. JENA and K. M. GUPTA, *J Power Sour* **80** (1999) 46.
27. X. CHEN and D. PENUMADU, *J Mater Res* (2006) in Review.
28. P. FORCHHEIMER, *Z. Ver. Deutsch, Ing.* **45** (1901) 1782.
29. K. VENKATARAMAN, W. T. CHOATE, E. R. TORRE and R. D. HUSUNG, *J Membr Sci* **39** (1988) 259.
30. O. SLOCOVA, H. SNAJDAUFOVA and P. SCHNEIDER, *Microp Mesop Mater* **65** (2003) 209.